

VOIC: Visible–Occluded Integrated Guidance for 3D Semantic Scene Completion

Zaidao Han, Risa Higashita, Jiang Liu, *Senior Member, IEEE*

Abstract—Camera-based 3D Semantic Scene Completion (SSC) is a critical task for autonomous driving and robotic scene understanding, aiming to infer a complete 3D volumetric representation of both semantics and geometry from a single image. Existing methods typically focus on end-to-end 2D-to-3D feature lifting and voxel completion, yet they often overlook the interference between high-confidence visible-region perception and low-confidence occluded-region reasoning caused by single-image input, which can lead to feature dilution and error propagation. To address these challenges, we introduce an offline Visible Region Label Extraction (VRLE) strategy that explicitly separates and extracts voxel-level supervision for visible regions from dense 3D ground truth, thereby purifying the supervisory space for the two complementary sub-tasks of visible-region perception and occluded-region reasoning. Building upon this, we propose the Visible–Occluded Interactive Completion Network (VOIC), a novel dual-decoder framework that explicitly decouples SSC into visible-region semantic perception and occluded-region scene completion. VOIC first constructs a base 3D voxel representation by fusing image features with depth-derived occupancy. The Visible Decoder then focuses on generating high-fidelity geometric and semantic priors, while the Occlusion Decoder leverages these priors along with cross-modal interaction to perform coherent global scene reasoning. Extensive experiments on the SemanticKITTI and SSCBench-KITTI360 benchmarks demonstrate that VOIC outperforms existing single-view image SSC methods in both geometric completion and semantic segmentation accuracy, achieving state-of-the-art performance. The code and pre-trained models are available at: <https://github.com/dzrdzrdzr/VOIC>.

Index Terms—Semantic Scene Completion, Visible-Occluded Decoupling, Autonomous Driving, Visible Region Label Extraction

I. INTRODUCTION

3D Semantic Scene Completion (SSC) aims to infer the complete 3D geometry and semantic structure of a scene from partial visual observations, such as monocular or stereo images. As a fundamental task in scene understanding, SSC provides dense and structured 3D representations of the surrounding environment, serving as a crucial bridge between

This work was supported in part by the National Key R&D Program of China (No. 2024YFE0198100) and the Shenzhen Medical Research Funds (Grant No. D2402014).

Zaidao Han and Risa Higashita are with the Research Institute of Trustworthy Autonomous Systems, Southern University of Science and Technology, Shenzhen 518055, China, and also with the Department of Computer Science and Engineering, Southern University of Science and Technology, Shenzhen 518055, China (emails: 12445017@mail.sustech.edu.cn; risa@mail.sustech.edu.cn).

Jiang Liu is with the Research Institute of Trustworthy Autonomous Systems, and the Department of Computer Science and Engineering, Southern University of Science and Technology, Shenzhen 518055, China; the School of Computer Science, University of Nottingham Ningbo China, Ningbo 315100, China; and the Department of Electronic and Information Engineering, Changchun University, Changchun 130022, China (email: liuj@sustech.edu.cn).

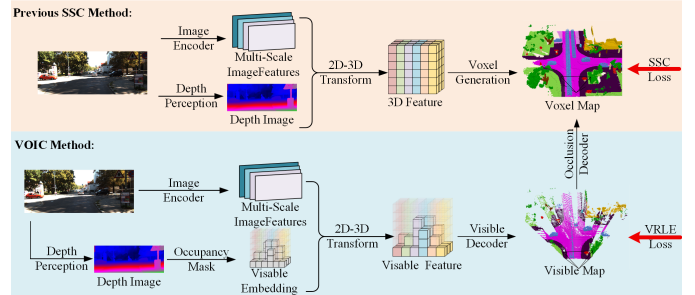


Fig. 1. Overview of the proposed VOIC framework. Unlike conventional SSC methods that supervise with full 3D labels, VOIC employs a decoupled progressive pipeline with intermediate supervision. 2D features are first lifted to 3D via cross-modal fusion. The Visible Decoder (VD) handles observed regions, and the Occlusion Decoder (OD) leverages normalized VD features as priors to reconstruct the full 3D scene. VD and OD are supervised with VRLE labels and global labels, respectively, ensuring accurate and stable completion.

perception and reconstruction. Accurate SSC is critical for numerous downstream applications, including autonomous driving, robotic navigation, and mixed reality [1]–[3].

Traditional LiDAR-based SSC methods [2], [4], [5] achieve high geometric accuracy due to high-quality 3D sensors. However, they suffer from high sensor costs, sparse points at long distances, and limited scalability for large-scale deployment. These limitations have driven research on camera-based SSC, which leverages dense image information to recover high-resolution 3D geometry and semantics without relying on expensive hardware [1].

Most existing vision-based SSC methods follow a standard pipeline: first extract 2D features, then project to 3D voxels, and finally decode the voxels. In this paradigm, 2D features extracted by a backbone network are lifted into the 3D voxel space, and decoders predict occupancy and semantic labels. To reduce depth ambiguity, many methods introduce auxiliary depth estimation [6], [7] to provide coarse geometric priors within the camera frustum. Despite these advances, single-view SSC remains highly challenging due to severe occlusions, complex spatial dependencies, and uneven information density between visible and occluded regions.

It is noteworthy that many vision-based Semantic Scene Completion (SSC) methods rely on multi-frame sequences to extend the coverage of occluded areas, thereby reducing the difficulty of predicting hidden geometry. In contrast, SSC with single-view image input lacks temporal redundancy, which significantly increases the ill-posedness of accurately reconstructing occluded voxels.

Existing methods, such as MonoScene [1] and VoxFormer [6], typically treat all voxels in a uniform manner, overlooking the intrinsic physical distinctions between observed and unobserved regions. Although a concurrent work, VisHall3D

[8], attempts to separate visible-region reconstruction from occluded-region completion at the structural level, it fundamentally lacks an explicit and differentiated supervision mechanism. Consequently, it fails to address the risk where visible-region supervision potentially contaminates the global completion process.

To address this challenge, we propose VOIC, which introduces the Visible Region Label Extraction (VRLE) strategy to provide explicit and targeted supervision signals for the visible decoder. This approach ensures that perceived features remain pure and stable, achieving a synergistic decoupling across both structural and supervisory dimensions. VRLE generates visible voxel labels from complete 3D annotations, enabling a clear distinction between visible and occluded voxels and providing structured guidance for subsequent completion.

Building upon VRLE, VOIC employs a dual-decoder architecture: the Visible Decoder (VD) is supervised by VRLE-generated labels to precisely reconstruct the geometry and semantics of observed voxels; the Occlusion Decoder (OD) collaborates with the VD by utilizing normalized visible features as spatial-semantic priors. Furthermore, the OD provides global contextual feedback to optimize visible-region predictions while holistically inferring the entire scene to generate final complete voxel predictions. Notably, VOIC relies strictly on single-view image input and does not depend on historical frames or multi-view information.

To achieve high-precision geometric priors and effective feature interaction, VOIC integrates multi-level positional encoding and adaptive feature interaction modules. During the 3D projection stage, the Visible Embedding Feature Constructor (VEFC) injects spatial geometric information into 2D features. Through a dynamic learnable sampling mechanism, VEFC mitigates feature dilution caused by depth estimation errors inherent in traditional projection methods.

Extensive experiments on SemanticKITTI [9] and SSCBench-KITTI-360 [10] demonstrate that VOIC consistently outperforms existing vision-based SSC methods across multiple metrics, achieving state-of-the-art performance in geometric completion and semantic consistency. It is worth noting that while VOIC achieves state-of-the-art performance, it still faces the inherent challenges of monocular perception, particularly in resolving depth ambiguities of complex articulated objects from a single viewpoint. The main contributions of this work are summarized as follows:

- 1) We propose VOIC, a novel single-view SSC framework that incorporates an offline Visible Region Label Extraction (VRLE) strategy to distinguish between visible and occluded voxels. This strategy facilitates a dual-decoder architecture—comprising a Visible Decoder (VD) and an Occlusion Decoder (OD)—to perform collaborative reasoning: the VD establishes robust visible priors under explicit VRLE supervision, while the OD leverages these priors alongside global supervision to infer the complete scene.
- 2) We introduce the Visible Embedding Feature Constructor (VEFC) and multi-level positional encoding mechanism to systematically enhance voxel feature geometric discriminability and semantic alignment, providing a

solid geometric foundation for VD/OD collaborative reasoning.

- 3) We conduct extensive experiments on SemanticKITTI and SSCBench-KITTI-360 to validate the effectiveness of VOIC. Results demonstrate superior performance over existing single-view SSC methods.

II. RELATED WORK

3D Semantic Scene Completion (SSC) aims to infer a complete volumetric representation of a scene, encompassing both the geometric structure and semantic labels of observed and occluded regions. Existing methods can be broadly categorized into those relying on native 3D sensor inputs and those adopting a vision-centric approach.

A. 3D Input-based Approaches

Early SSC methods leveraged native 3D data for high-fidelity reconstruction. The pioneering work, SSCNet [11], introduced SSC for indoor RGB-D scenes. Subsequent methods, such as 3DSketch [12], the approach by Li et al. [13], and the Cascaded Context Pyramid Network (CCPNet) [14], adopted the Truncated Signed Distance Function (TSDF) to better guide the prediction of geometry and semantics.

The emergence of large-scale outdoor datasets, such as SemanticKITTI [9] and OpenOccupancy [15], subsequently catalyzed the development of methods tailored for outdoor environments. A common strategy in this domain is to directly process LiDAR point clouds. For instance, LMSCNet [16] utilizes a 2D UNet to extract Bird’s-Eye View (BEV) features from sparse scans, which are then unrolled along the height dimension to complete the 3D scene. JS3C-Net [17] proposes a sparse single-sweep segmentation framework with contextual shape priors and leverages multi-frame LiDAR aggregation to convert sparse scans into dense representations.

To leverage complementary information from images and LiDAR, recent methods focus on multi-modal fusion. Chang et al. [18] address unreliable image features and modality trade-offs by introducing a weakly-supervised loss, attention-based feature fusion, and confidence-aware late fusion. IPVoxelNet [19] maps images and point clouds into a unified voxel space, independently learns geometric and semantic features, and uses cross-modal knowledge distillation to enhance scene understanding.

While 3D input-based methods achieve remarkable accuracy, their dependency on expensive sensors like LiDAR limits practical scalability. This constraint has motivated a parallel line of research into vision-centric methods, which seek to infer complete 3D scenes from low-cost, readily available monocular or multi-view images.

B. Visual-Centric Approaches

Vision-centric SSC methods address the challenge of reconstructing 3D scenes from images. The single-image SSC pipeline was largely established by MonoScene [1], which lifts 2D image features into a 3D frustum to generate dense voxel representations. Early innovations primarily focused on

enhancing the 3D decoder: OccFormer [20] provides efficient, long-range encoding for voxel features; NDC-scene [21] projects 2D features into Normalized Device Coordinate (NDC) space to recover depth; and TPVFormer [22] represents 3D space with tri-perspective views and uses Transformers to capture spatial dependencies. HASSC [23] tackles the class imbalance issue via a hard sample-aware training strategy that dynamically selects challenging voxels for refinement.

A core challenge in single-image SSC is depth ambiguity. VoxFormer [6] systematically addresses this by first generating sparse depth estimates and then using deformable attention to propagate and densify contextual features. Beyond geometry, instance-level reasoning has also been integrated to boost performance. Symphonies [7] employs serial instance propagation attention to model instance semantics and reduce occlusion errors, while Xiao et al. [24] propose an instance-aware framework that fuses mask-derived cues via a dedicated attention module.

The field has recently seen significant advances through multi-modal fusion and temporal modeling. MiXSSC [25] combines sparse features from forward projection with dense depth priors from backward projection. HTCL [26] introduces hierarchical temporal context learning for better consistency, CurriFlow [27] leverages optical flow and curriculum learning, and CF-SSC [28] extends the perceptual range via pseudo-future frame prediction.

Architectural innovations continue to push the boundaries. FoundationSSC [29] uses stereo (binocular) input and proposes a dual-decoupling framework for separate semantic and geometric refinement. MVFormer [30] utilizes a UNet-like decoder with Mix-Voxel attention, VFG-SSC [31] adopts a semi-supervised approach to leverage 2D foundation models, SPHERE [32] jointly models semantics and physics with voxels and Gaussians, and MARE [33] introduces a memory bank to complete unseen regions. VisHall3D [8] introduces a ‘‘Vision vs. Hallucination’’ strategy to separate visible-region reconstruction from occluded-region completion, but this separation is primarily at the model form level and does not fundamentally decouple supervision for visible and occluded voxels.

In summary, while many vision-centric methods mitigate occlusion by leveraging multi-frame temporal redundancy, such approaches do not address the fundamental issue of supervision ambiguity in single-image settings. To bridge this gap, we propose VOIC, which explicitly reformulates the task through a supervisory decoupling strategy. By introducing distinct learning objectives for ‘‘visible region perception’’ and ‘‘occluded region prediction,’’ our method effectively rectifies supervision contamination, enabling structured and high-fidelity scene completion from a single-view image without relying on historical data.

III. METHODOLOGY

A. Overview

We introduce VOIC, a unified framework designed to address a critical yet underexplored issue in monocular 3D Semantic Scene Completion (SSC): inaccurate supervision

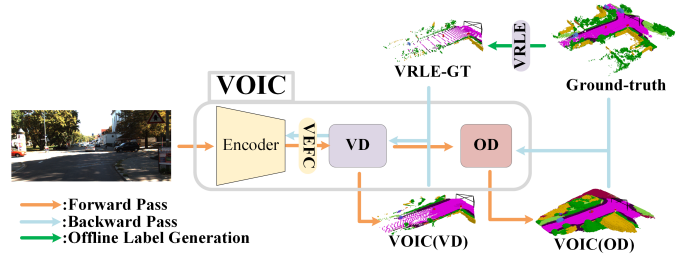


Fig. 2. Overall framework of the proposed method. During training, the input image is processed by the backbone and VEFC module. The Visible Decoder (VD) predicts visible voxels, while the Occlusion Decoder (OD) predicts occluded voxels. The VRLE-tag is generated offline from the ground truth (GT) using the VRLE process. The VD prediction is supervised by the VRLE-tag, and the OD prediction is supervised by the GT. The losses are computed and optimized via backpropagation. During inference, only the forward pass is performed.

on visible regions can systematically degrade global scene completion. Formally, given a single RGB image $I^{rgb} \in \mathbb{R}^{H_{img} \times W_{img} \times 3}$ as input, the objective is to predict the complete scene geometry and semantics $\hat{\mathbf{Y}}$, which approximates the ground truth $\mathbf{Y} \in \mathbb{R}^{X \times Y \times Z \times N_c}$. This is formulated as learning a network Θ such that $\hat{\mathbf{Y}} = \Theta(I^{rgb})$.

To facilitate this decoupled learning paradigm, our framework incorporates a dual supervision mechanism:

- 1) **Explicit Visibility Supervision:** Derived via an offline Visible Region Label Extraction (VRLE) strategy (Sec. III-B), this supervision guides the network to capture precise features of observable surfaces.
- 2) **Holistic Scene Supervision:** Utilizing the complete ground-truth annotations, this forces the network to infer occluded regions based on the established visible priors.

The overall computational pipeline is illustrated in Figure 2. VRLE-generated labels provide supervision for the Visible Decoder (VD), while global ground-truth labels supervise the Occlusion Decoder (OD). During the forward pass, as illustrated in Figure 3, the pipeline first employs the Visible Embedding Feature Constructor (VEFC) (Sec. III-C) to lift 2D image features into a 3D volumetric representation. Specifically, VEFC leverages a ResNet-50 backbone [34] and a DETR-style attention module [35] to strengthen the coupling between image cues and 3D occupancy.

These 3D features are subsequently processed by the Visible Decoder (VD) (Sec. III-D) to reconstruct the geometry and semantics of observable surfaces under visibility supervision. Building upon VD’s high-fidelity predictions, the Occlusion Decoder (OD) (Sec. III-E) uses these results as spatial-semantic priors to infer the complete 3D scene under holistic supervision, ensuring a coherent reconstruction. Finally, a segmentation head with an ASPP module [36] produces the final per-voxel semantic predictions.

B. Visible Region Label Extraction (VRLE)

Standard SSC datasets (e.g., SemanticKITTI [9]) provide complete 3D semantic annotations but inherently lack explicit distinctions between visible and occluded voxels. This uniform supervision fails to account for the fundamentally

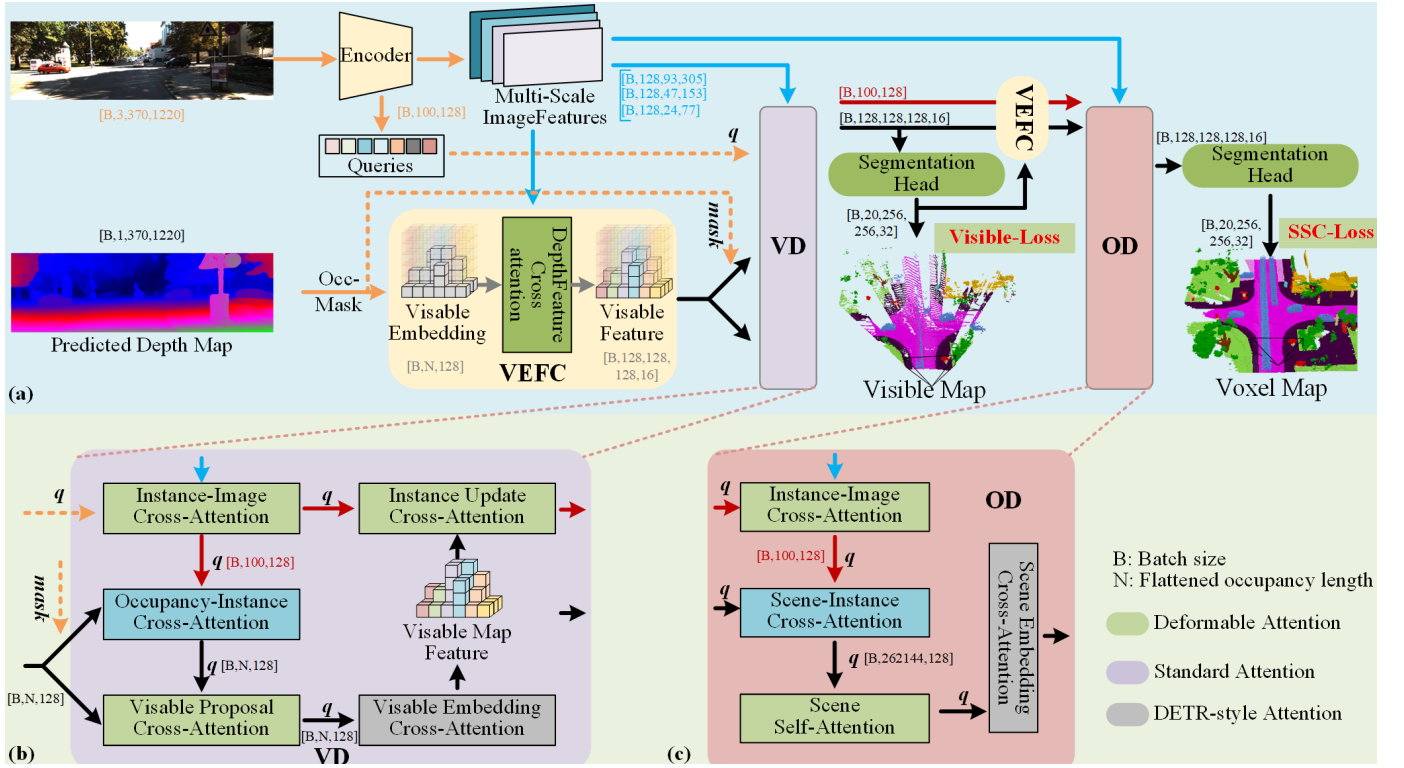


Fig. 3. Overall architecture of the VOIC framework. (a) The model follows a progressive visible-occluded paradigm that decouples the 3D SSC task with differentiated supervision. The Visible Embedding Feature Constructor (VEFC) lifts 2D image features into 3D and fuses them with depth-derived occupancy to form a unified volumetric representation. (b) The Visible Decoder (VD) predicts geometry and semantics of observed regions under explicit visible-voxel supervision. (c) The Occlusion Decoder (OD) leverages normalized visible features as spatial-semantic priors and reconstructs the full 3D scene under global scene completion supervision.

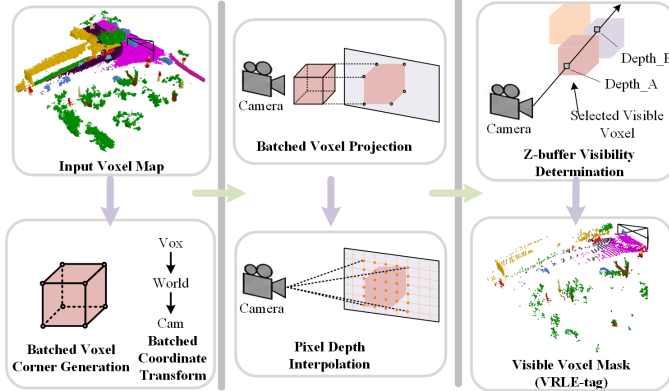


Fig. 4. Overview of VRLE module.

different nature of visible perception versus occluded reasoning. To solve this, we introduce VRLE, an offline label generation strategy that provides unambiguous supervision for the proposed Visible Decoder by performing a visibility-aware projection. The computational process is illustrated in Figure 4. The VRLE process begins with *Voxel Instantiation and Geometric Projection*. Given the complete ground-truth semantic voxel grid $\mathbf{Y} \in \mathbb{R}^{X \times Y \times Z \times N_c}$, we first extract the set of occupied voxels $\mathcal{V} = \{v_i \mid \mathbf{Y}_i \neq \text{empty}\}$. N_c denotes the number of semantic classes including the empty class. For each voxel v_i , we define its structure by eight vertices $\mathcal{P}_i^{\text{vox}} \in \mathbb{R}^{8 \times 3}$. Since visibility is determined by the voxel's actual surfaces rather than its center, representing each voxel with eight vertices allows explicit modeling of surface-level occlusion. To simulate the imaging process and establish

correspondence between the 3D voxel structure and the 2D input image, each voxel vertex $\mathbf{p}_k^{\text{vox}}$ is transformed to the camera coordinate system and then projected onto the image plane using the standard pin-hole camera model. This pipeline uses the voxel-to-world transformation $\mathbf{T}_{v \rightarrow w}$, the camera extrinsic parameters $[\mathbf{R} | \mathbf{t}]$, and the intrinsic matrix \mathbf{K} , and is formally defined as:

$$\begin{aligned} \mathbf{p}_k^{\text{world}} &= \mathbf{T}_{v \rightarrow w} \mathbf{p}_k^{\text{vox}} \\ \mathbf{p}_k^{\text{cam}} &= \mathbf{R} \mathbf{p}_k^{\text{world}} + \mathbf{t} \end{aligned} \quad (1)$$

$$u = \text{round}\left(f_x \frac{x}{z} + c_x\right), \quad v = \text{round}\left(f_y \frac{y}{z} + c_y\right),$$

where $\mathbf{p}_k^{\text{cam}} = [x, y, z]^T$ denotes the point in the camera coordinate frame, f_x, f_y are the focal lengths, and (c_x, c_y) is the principal point. The projected vertices form a 2D polygon Π_i corresponding to voxel v_i .

Identifying truly visible voxels requires eliminating depth ambiguity due to occlusions. Since traditional ray-casting is prohibitively slow for dense voxel grids, we employ a *Vectorized Sparse Rasterization pipeline enhanced with Z-buffering*. For computational efficiency, we first perform *Sparse Bounding-Box Sampling*: for each projected voxel Π_i , we compute its 2D Axis-Aligned Bounding Box (AABB) \mathcal{B}_i and generate a sparse grid of candidate pixels \mathcal{S}_i within \mathcal{B}_i using a sampling stride δ (e.g., $\delta = 4$). Next, in the *Inclusion Verification and Depth Interpolation* stage, we decompose the cube's projected volume into its six quadrilateral faces. A vectorized cross-product test is employed to determine if

a candidate pixel $p \in \mathcal{S}_i$ falls within any projected face. For every validated pixel p , we calculate its precise depth d_p through robust linear interpolation of the face vertices' depths, explicitly handling degenerate projection cases to ensure numerical stability. We maintain a global depth buffer $\mathcal{Z} \in \mathbb{R}^{H_{img} \times W_{img}}$ to record the minimum depth. The visibility mask is generated by the following rule: a voxel v_i is marked as visible if its depth is the smallest at any covered pixel location (u, v) :

$$v_i \in \mathcal{V}_{vis} \iff \exists(u, v) \in \Pi_i, \text{ s.t. } d_{u,v}^{(i)} = \min_{j \in \mathcal{V}}(d_{u,v}^{(j)}), \quad (2)$$

where $d_{u,v}^{(j)}$ is the interpolated depth of voxel v_j at pixel (u, v) . Finally, VRLE produces a binary visibility mask $\mathbf{M}_{vis} \in \{0, 1\}^{X \times Y \times Z}$. The ground truth is then strategically decoupled to derive the visible targets $\mathbf{Y}_{vis} = \mathbf{Y} \odot \mathbf{M}_{vis}$. These \mathbf{Y}_{vis} provide dedicated supervision for the Visible Decoder, while the complete ground truth \mathbf{Y} is used to supervise the final prediction of the Occlusion Decoder, ensuring holistic scene understanding.

C. Visible Embedding Feature Constructor (VEFC)

First, using the predicted depth map \mathbf{D}_{pre} obtained from the depth prediction module, we transform pixel coordinates into world coordinates through the camera parameters to construct a binary occupancy mask $\mathbf{M} \in \{0, 1\}^{X \times Y \times Z}$ within the 3D voxel space. This mask is activated only at voxel locations intersected by the projected depths, effectively filtering out uninformative free space.

For the valid voxels indicated by the mask \mathbf{M} , we initialize their content features $\mathbf{Q}_{content}$ as zero vectors. These zero vectors are then fused with the image features \mathbf{F}_{2D} , where $\mathbf{F}_{2D} = \text{Backbone}(I^{rgb})$, through a Deformable Attention module (DeformAttn) [35]. In this process, the 3D geometric positional embedding \mathbf{S}_{pos} is added to the content-free queries to form positional queries, which guide the attention mechanism to attend to the corresponding regions in the image features.

$$\mathbf{F}_{voxel} = \text{DeformAttn}(\mathbf{Q}_{content} + \mathbf{S}_{pos}, \mathcal{P}(\mathbf{S}_{pos}), \mathbf{F}_{2D}) \quad (3)$$

where \mathcal{P} denotes the 3D-to-2D projection function. In the Deformable Attention module, the voxel queries—augmented with geometric positional encoding—attend to their corresponding regions in the image feature map. This mechanism ensures that the resulting voxel features are directly grounded in the explicit correspondence between 3D geometry and image appearance under the current view, thereby preventing the “hallucinated” responses that often arise from free-form learnable queries in occluded or complex areas. Finally, the generated sparse features are scattered back into the dense blank grid to form the initial scene embedding.

D. Visible Decoder (VD)

As illustrated in Fig. 3(b), the Visible Decoder (VD) serves as the primary component for achieving high-fidelity semantic perception within the visible regions. The comprehensive data flow and feature transformation procedures are formally summarized in Algorithm 1.

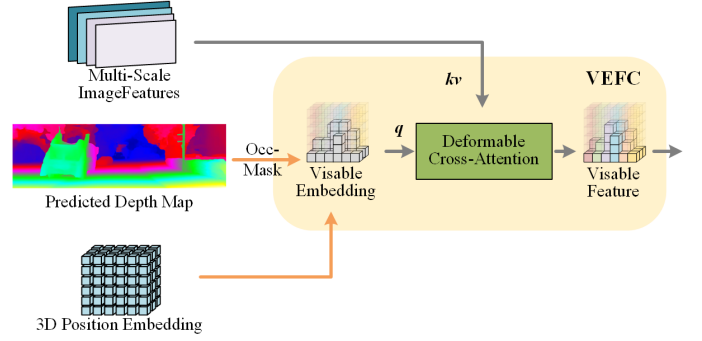


Fig. 5. Sparse Voxel Feature Initialization. The VEFC module creates a geometry-driven 3D representation using a zero-initialized query. An occupancy mask sparsifies the structure, while 3D positional encoding enables precise localization. Deformable Attention then aggregates 2D image features into the visible voxels.

The VD architecture is designed to balance computational efficiency with structural robustness through a multi-stage integration paradigm. First, to mitigate the memory overhead associated with high-resolution multi-scale image features \mathbf{F}_{2D} , we employ a set of instance queries \mathbf{Q}_{inst} to compress and aggregate the most salient visual cues. These compressed queries subsequently interact with the critical voxels identified by the occupancy mask \mathbf{M} through the *Occupancy-Instance Cross Attention* mechanism. This step facilitates the explicit fusion of image-derived semantics with the skeleton of the 3D geometric structure.

Considering that the initial occupancy mask \mathbf{M} —derived from depth estimation—may contain inherent inaccuracies or misalignments, we incorporate a structural refinement strategy. The sparse features obtained from the masked interaction are re-integrated with the holistic (unmasked) voxel features $\text{Flatten}(\mathbf{F}_{vis})$, where \mathbf{F}_{vis} is initialized from the VEFC output \mathbf{F}_{voxel} and represents the full visible-region voxel representation. By leveraging the global 3D scene context, this process effectively compensates for potential errors in the mask, ensuring spatial consistency across the observable volume. To further enrich the categorical representation, the resulting features are fused with class embedding priors \mathbf{C}_{vd} via a DETR-style attention module, yielding the final visible-region output features \mathbf{F}_{vis}^{VD} .

A key characteristic of our design is the reciprocal guidance between the scene features and the queries. Since \mathbf{F}_{vis}^{VD} encapsulates refined occupancy information and semantic priors, it is utilized to update the instance queries \mathbf{Q}'_{inst} through 3D Deformable Attention. This feedback loop ensures that the updated queries \mathbf{Q}'_{inst} carry explicit 3D-aware constraints. Consequently, in the subsequent Occlusion Decoder (OD), these queries can establish more precise correspondences with image features, providing superior guidance for reasoning within the unobserved spaces.

E. Occlusion Decoder (OD)

The Occlusion Decoder (OD) is designed to reconstruct the complete 3D scene by propagating structural and semantic priors from the visible regions into the unobserved spaces. The

Algorithm 1 Forward Pass of the Visible Decoder (VD)

Require: Initial 3D embedding for VD from VEFC \mathbf{F}_{vis} (Shape: $B \times C \times X \times Y \times Z$), 2D multi-scale image features \mathbf{F}_{2D} , Instance queries \mathbf{Q}_{inst} (Shape: $B \times N_q \times C$), Occupancy mask \mathbf{M} , 2D instance reference points \mathbf{R}_{2D} , Class embeddings \mathbf{C}_{vd} .

Ensure: Refined visible features $\mathbf{F}_{\text{vis}}^{\text{VD}}$, Updated instance queries $\mathbf{Q}'_{\text{inst}}$.

- 1: // **Step 1: Instance-Image Grounding**
- 2: Flatten \mathbf{F}_{2D} into 1D sequences;
- 3: $\mathbf{Q}'_{\text{inst}} \leftarrow \text{DeformAttn}(\mathbf{Q}_{\text{inst}}, \mathbf{R}_{2D}, \mathbf{F}_{2D})$; \triangleright Instance-Image Cross-Attn, output shape: $B \times N_q \times C$
- 4: // **Step 2: Visible Feature Extraction (Sparsification)**
- 5: $\mathbf{E}_{\text{vis}}^{\text{flat}} \leftarrow \text{Flatten}(\mathbf{F}_{\text{vis}})[\mathbf{M}]$; \triangleright Output: $B \times N \times C$, N is valid voxels
- 6: // **Step 3: Multi-stage Feature Refinement**
- 7: $\mathbf{E}_{\text{vis}}^{\text{flat}} \leftarrow \text{CrossAttn}(\mathbf{E}_{\text{vis}}^{\text{flat}}, \mathbf{Q}'_{\text{inst}})$; \triangleright Occupancy-Instance Cross-Attn
- 8: $\mathbf{E}_{\text{vis}}^{\text{flat}} \leftarrow \text{DeformAttn}(\mathbf{E}_{\text{vis}}^{\text{flat}}, \mathbf{R}_{3D}, \text{Flatten}(\mathbf{F}_{\text{vis}}))$; \triangleright Visible Proposal Cross-Attn
- 9: $\mathbf{E}_{\text{vis}}^{\text{final}} \leftarrow \text{CrossAttn}(\mathbf{E}_{\text{vis}}^{\text{flat}}, \mathbf{C}_{\text{vd}})$; \triangleright Visible Embedding Cross-Attn
- 10: // **Step 4: Spatial Reconstruction & Query Update**
- 11: $\mathbf{F}_{\text{vis}}^{\text{VD}} \leftarrow \text{IndexBack}(\mathbf{0}, \mathbf{E}_{\text{vis}}^{\text{final}}, \mathbf{M})$; \triangleright Scatter sparse features onto a zero-initialized grid
- 12: $\mathbf{Q}_{\text{inst}}^{\text{VD}} \leftarrow \text{DeformAttn}(\mathbf{Q}'_{\text{inst}}, \mathbf{R}_{3D}, \text{Flatten}(\mathbf{F}_{\text{vis}}^{\text{VD}}))$; \triangleright Instance Update Cross-Attn
- 13: **return** $\mathbf{F}_{\text{vis}}^{\text{VD}}, \mathbf{Q}_{\text{inst}}^{\text{VD}}$

core intuition of the OD lies in leveraging the high-confidence visible-region features to guide the reasoning of hidden structures through a multi-stage feature evolution paradigm.

First, to enhance the semantic understanding of the queries, the instance queries $\mathbf{Q}_{\text{inst}}^{\text{VD}}$ derived from the VD—which already encapsulate preliminary 3D spatial awareness—are re-fused with the multi-scale image features \mathbf{F}_{2D} through *Instance-Image Cross-Attention*. By re-grounding the queries in the image plane, the model strengthens its grasp of the object-level semantics before initiating 3D completion. Simultaneously, the refined visible-region features $\mathbf{F}_{\text{vis}}^{\text{VD}}$ are injected back into the holistic grid via the *IndexBack* operation using the occupancy mask \mathbf{M} . This ensures that the established visible priors serve as fixed anchors within the integrated representation \mathbf{E}_{occ} , providing reliable spatial guidance for the subsequent completion process.

Subsequently, the OD achieves cross-modal integration by fusing the image-enhanced queries $\mathbf{Q}_{\text{inst}}^{\text{OD}}$ with the initial 3D grid \mathbf{E}_{occ} through *Scene-Instance Cross-Attention*. To further solidify the feature representation, a *Scene Self-Attention* mechanism is employed. By performing deformable spatial reasoning over the entire volume, the model enhances the internal expressive power of the features, allowing structural cues to propagate seamlessly from observable boundaries to occluded regions.

Finally, the categorical expressive capability is augmented by the *Scene Embedding Cross-Attention* stage. Here, a specialized set of class-level embeddings \mathbf{C}_{od} interacts with the

Algorithm 2 Feature Propagation in Occlusion Decoder (OD)

Require: Initial 3D embedding for OD from VEFC \mathbf{F}_{occ} , Visible-refined features $\mathbf{F}_{\text{vis}}^{\text{VD}}$, Instance queries $\mathbf{Q}_{\text{inst}}^{\text{VD}}$, 2D image features \mathbf{F}_{2D} , Occupancy mask \mathbf{M} , 3D voxel positions \mathbf{R}_{3D} , Class embeddings \mathbf{C}_{od} .

Ensure: Holistic refined features $\mathbf{F}_{\text{occ}}^{\text{OD}}$.

- 1: // **Stage 1: Semantic Re-grounding**
- 2: $\mathbf{Q}_{\text{inst}}^{\text{OD}} \leftarrow \text{DeformAttn}(\mathbf{Q}_{\text{inst}}^{\text{VD}}, \mathbf{R}_{2D}, \mathbf{F}_{2D})$; \triangleright Instance-Image Cross-Attn
- 3: // **Stage 2: Prior Injection & Spatial Mapping**
- 4: $\mathbf{E}_{\text{occ}} \leftarrow \text{IndexBack}(\mathbf{F}_{\text{occ}}, \mathbf{F}_{\text{vis}}^{\text{VD}}, \mathbf{M})$; \triangleright Inject VD priors into the OD grid
- 5: $\mathbf{E}_{\text{occ}}^{\text{flat}}$, shape $\leftarrow \text{Flatten}(\mathbf{E}_{\text{occ}})$;
- 6: // **Stage 3: Progressive Feature Evolution**
- 7: $\mathbf{E}_{\text{occ}}^{\text{flat}} \leftarrow \text{CrossAttn}(\mathbf{E}_{\text{occ}}^{\text{flat}}, \mathbf{Q}_{\text{inst}}^{\text{OD}})$; \triangleright Scene-Instance Cross-Attn
- 8: $\mathbf{E}_{\text{occ}}^{\text{flat}} \leftarrow \text{DeformAttn}(\mathbf{E}_{\text{occ}}^{\text{flat}}, \mathbf{R}_{3D}, \mathbf{E}_{\text{occ}}^{\text{flat}})$; \triangleright Geometric completion via Self-Attn
- 9: // **Stage 4: Category-Level Augmentation**
- 10: $\mathbf{E}_{\text{occ}}^{\text{final}} \leftarrow \text{CrossAttn}(\mathbf{E}_{\text{occ}}^{\text{flat}}, \mathbf{C}_{\text{od}})$; \triangleright Scene Embedding Cross-Attn
- 11: $\mathbf{F}_{\text{occ}}^{\text{OD}} \leftarrow \text{Reshape}(\mathbf{E}_{\text{occ}}^{\text{final}}, \text{shape})$; \triangleright Restore to 3D volume
- 12: **return** $\mathbf{F}_{\text{occ}}^{\text{OD}}$

refined voxel features via a DETR-style decoupled attention module. This process fuses global scene priors with high-dimensional category information, ensuring that the completed scene is both geometrically consistent and semantically plausible. The OD ultimately outputs the fully refined voxel features $\mathbf{F}_{\text{occ}}^{\text{OD}}$, which are then passed to the segmentation head for the final holistic scene prediction.

F. Loss Functions

VOIC learns visible and occluded scene representations via two supervision branches: the Visible Decoder (VD) and the Occlusion Decoder (OD). The overall training objective is defined as:

$$L_{\text{total}} = L_{\text{VD}} + L_{\text{OD}}. \quad (4)$$

Both decoders share the same objective that jointly supervises geometric occupancy and semantic prediction:

$$L_X = \lambda_{\text{scal}} L_{\text{scal}}^{\text{geo}} + \lambda_{\text{ce}} L_{\text{ce}} + \lambda_{\text{mIoU}} L_{\text{mIoU}}, \quad (5)$$

where $X \in \{\text{VD}, \text{OD}\}$. $L_{\text{scal}}^{\text{geo}}$ follows MonoScene [1] and L_{ce} is the voxel-wise cross-entropy loss used in Symphonize3D [7]. λ_{scal} , λ_{ce} , and λ_{mIoU} denote weighting coefficients.

To better align optimization with the evaluation metric, a differentiable semantic mIoU loss is adopted. Let Ω denote the set of valid voxels (excluding ignore labels) within the holistic grid $\mathbb{R}^{X \times Y \times Z}$. For each voxel $i \in \Omega$, let $\hat{y}_{i,c}$ and $y_{i,c}$ denote the predicted probability and the one-hot ground-truth label for class c , respectively. The soft IoU for class c is defined as:

$$\text{IoU}_c = \frac{\sum_{i \in \Omega} \hat{y}_{i,c} y_{i,c}}{\sum_{i \in \Omega} \hat{y}_{i,c} + \sum_{i \in \Omega} y_{i,c} - \sum_{i \in \Omega} \hat{y}_{i,c} y_{i,c}}, \quad (6)$$

where $c \in \{1, \dots, N_c - 1\}$ (excluding the empty category).

The final mIoU loss is formulated as:

$$L_{\text{mIoU}} = 1 - \frac{1}{N_c - 1} \sum_{c=1}^{N_c-1} \text{IoU}_c, \quad (7)$$

IV. EXPERIMENTS

In this section, we present the experimental evaluations of our proposed method on the SemanticKITTI [9] and SSCBench-KITTI-360 [10] datasets. Comparative results against existing state-of-the-art approaches are provided in Sec. IV-C, while comprehensive ablation studies are reported in Sec. IV-D to further analyze the effectiveness of each component.

A. Dataset and Metric

We conduct experiments on the SemanticKITTI [9] and SSCBench-KITTI-360 [10] datasets, both of which offer densely annotated urban driving scenes derived from the KITTI Odometry Benchmark. The scenes are voxelized into grids of size $256 \times 256 \times 32$, covering a spatial volume of $51.2\text{m} \times 51.2\text{m} \times 6.4\text{m}$ with a voxel size of 0.2 m.

SemanticKITTI contains 10 training sequences, 1 validation sequence, and 11 hidden test sequences. It provides RGB images with a resolution of 1226×370 and includes 20 semantic classes. SSCBench-KITTI-360 provides 7 training sequences, 1 validation sequence, and 1 test sequence, offering RGB images of size 1408×376 and defining 19 semantic classes.

We follow standard SSC evaluation protocols and report Intersection over Union (IoU) and mean IoU (mIoU). IoU assesses binary occupancy (empty vs. occupied) and reflects geometric reconstruction performance, whereas mIoU evaluates per-class semantic accuracy—the primary metric in most SSC benchmarks [1] [7] [6] [32].

B. Implementation Details

We train our model on two RTX A6000 GPUs with a batch size of 1. Random horizontal flipping [37] [38] [39] and color jittering (brightness in the range [1.2, 1.25], contrast in the range [0.6, 0.65], and saturation adjustment of 0.1) are applied as image augmentation methods.

Following previous methods [6]–[8], [30], [40], [41], we use MobileStereoNet[33] for depth prediction. During both training and inference, the model takes as input a single RGB image together with predicted depth map

Training is performed using the AdamW [42] optimizer with an initial learning rate of 3.5×10^{-4} , a weight decay of 0.015, and momentum coefficients $(\beta_1, \beta_2) = (0.9, 0.99)$. The loss weights for both VD and OD are set as $\lambda_{\text{scal}} = 1$, $\lambda_{\text{ce}} = 1$, and $\lambda_{\text{miou}} = 10$.

Following other comparable methods [33] [7], the ResNet-50 [43] backbone and image encoder are initialized with pre-trained MaskDINO [34] weights.

A MultiStepLR scheduler is adopted, where the learning rate is decayed by a factor of 0.1 at epochs 12 and 15. The total training length is 16 epochs.

We set the input spatial voxel size to $128 \times 128 \times 16$ with $C = 128$ channels. The voxel representation is upsampled to $256 \times 256 \times 32$ using a 3D transposed convolution.

C. Main Results

Quantitative Results Table I presents a comparison of our proposed VOIC with other state-of-the-art camera-based SSC methods on the SemanticKITTI hidden test set. VOIC outperforms existing approaches, establishing a new state-of-the-art. Compared to CGFormer, which also takes single-view images as input, our method achieves improvements of 1.38% in mIoU and 0.81% in IoU. These results validate the effectiveness of our approach in both geometric and semantic aspects. Notably, VOIC delivers top-tier performance on long-tailed categories, such as car, truck, bicycle, and motorcycle.

To further evaluate the effectiveness of VOIC across diverse scenarios, as shown in Table II, our method demonstrates significant advantages in semantic and geometric analysis on the data-rich SSCBench-KITTI-360 benchmark. VOIC surpasses all published methods in mIoU metrics, achieving the best performance across the majority of categories.

Furthermore, as detailed in Table III, we compare the inference time and number of parameters with other state-of-the-art methods on the SemanticKITTI validation set. While achieving state-of-the-art performance with 18.06% mIoU, VOIC also features a shorter inference time and a more lightweight architecture, requiring only 45.4M parameters.

Qualitative Results To provide an intuitive demonstration of VOIC’s performance, Figure 6 illustrates qualitative results on the SemanticKITTI validation set, comparing our method with Symphonize. The first row shows the input images, ground truth labels, and VRLE-GT, while the second row presents the outputs of Symphonize and VOIC on OD and VD, respectively. It can be observed that VD closely follows VRLE-GT, achieving more accurate semantic segmentation and occupancy information on visible objects. For example, in the first case, VOIC effectively captures the position and details of small objects such as cars, while in the second case, it accurately predicts pedestrian locations and guides OD accordingly.

D. Ablation Studies

To better understand the contributions of different components in VOIC, we conducted a series of ablation experiments, focusing on three aspects: the architectural design, the choice of 2D-to-3D projection methods, and the interaction flow between the Visible Decoder (VD) and the Occlusion Decoder (OD). All results are benchmarked on the SemanticKITTI validation set.

Ablation on the Architectural Components and Projection Method. Table IV summarizes the performance of VOIC under different architectural configurations. We first construct a Baseline model by removing the VRLE label, adopting FLoSP [1] as the 2D-to-3D projection module, and using OD as the final decoder, which yields 36.86% IoU and 11.09% mIoU.

Replacing FLoSP with the proposed VEFC module (Method 1), while still omitting VRLE and using only OD, improves performance to 44.88% IoU and 15.88% mIoU. This improvement arises from VEFC’s depth-aware feature aggregation,

TABLE I
QUANTITATIVE RESULTS ON THE SEMANTICKITTI HIDDEN TEST SET. ^T REPRESENTS THE USE OF MULTI-FRAME INPUT. [†] REPRESENTS THE USE OF MULTI-CAMERA IMAGES AS INPUT. THE BEST AND THE SECOND BEST RESULTS ARE MARKED IN **BOLD** AND UNDERLINED, RESPECTIVELY.

Method	IoU	mIoU	road (15.30%)	sidewalk (11.3%)	parking (1.12%)	other-ground (0.58%)	building (14.1%)	car (3.92%)	truck (0.16%)	bicycle (0.03%)	motorcycle (0.00%)	other-veh. (0.20%)	vegetation (9.9%)	trunk (0.51%)	terrain (9.17%)	person (0.07%)	bicyclist (0.07%)	motorcyclist (0.08%)	fence (3.90%)	pole (0.29%)	traf.-sign (0.08%)
MonoScene [1]	34.16	11.08	54.7	27.1	24.8	5.7	14.4	18.8	3.3	0.5	0.7	4.4	14.9	2.4	19.5	1.0	1.4	0.4	11.1	3.3	2.1
TPVFormer [†] [22]	34.25	11.26	55.1	27.2	27.4	6.5	14.8	19.2	3.7	1.0	0.5	2.3	13.9	2.6	20.4	1.1	2.4	0.3	11.0	2.9	1.5
VoxFormer ^T [6]	43.21	13.41	54.1	26.9	25.1	7.3	23.5	21.7	3.6	1.9	1.6	4.1	24.4	8.1	24.2	1.6	1.1	0.0	13.1	6.6	5.7
OccFormer [20]	34.53	12.32	55.9	30.3	31.5	6.5	15.7	21.6	1.2	1.5	1.7	3.2	16.8	3.9	21.3	2.2	1.1	0.2	11.9	3.8	3.7
NDC-Scene [21]	33.87	11.55	56.2	28.7	28.0	5.6	15.8	19.7	1.8	1.1	1.1	4.9	14.3	2.6	20.6	0.7	1.7	0.4	11.2	3.2	1.7
Symphonies [7]	42.19	15.04	58.4	29.3	26.9	11.7	24.7	23.6	3.2	3.6	2.6	5.6	24.2	10.0	23.1	<u>3.2</u>	1.9	<u>2.0</u>	16.1	7.7	8.0
SGN ^T [40]	<u>45.42</u>	15.76	60.4	31.4	28.9	8.7	28.4	25.4	4.5	0.9	1.6	3.7	27.4	12.6	28.4	0.5	0.3	0.1	18.1	10.0	8.3
MVFormer [30]	43.02	15.81	59.7	31.5	29.5	12.5	24.4	23.9	2.8	<u>3.7</u>	2.4	<u>6.2</u>	26.8	11.2	24.9	3.1	2.6	2.2	16.8	8.4	7.8
CGFormer [41]	44.41	16.63	64.3	34.2	<u>34.1</u>	12.1	25.8	26.1	4.3	3.7	1.3	2.7	24.5	11.2	<u>29.3</u>	1.7	<u>3.6</u>	0.4	18.7	8.7	<u>9.3</u>
HTCL ^T [26]	44.23	17.09	<u>64.4</u>	<u>34.8</u>	33.8	12.4	25.9	<u>27.3</u>	5.7	1.8	2.2	5.4	25.3	10.8	31.2	1.1	3.1	0.9	21.1	9.0	8.3
VisHall3D [8]	46.5	<u>17.46</u>	64.6	34.1	32.0	<u>12.5</u>	26.9	26.7	<u>7.5</u>	2.9	<u>3.3</u>	6.2	<u>27.3</u>	12.5	28.0	2.3	5.1	1.9	19.5	9.2	9.2
VOIC(proposed)	45.22	18.01	63.3	36.0	36.9	8.2	<u>27.5</u>	27.9	8.3	5.9	6.0	7.0	27.2	<u>12.6</u>	28.6	3.6	2.4	0.2	<u>20.9</u>	<u>9.8</u>	10.0

TABLE II
QUANTITATIVE RESULTS ON THE SSCBENCH-KITTI360 TEST SET. ^T REPRESENTS THE USE OF MULTI-FRAME INPUT. [†] REPRESENTS THE USE OF MULTI-CAMERA IMAGES AS INPUT. THE BEST AND THE SECOND BEST RESULTS ARE MARKED IN **BOLD** AND UNDERLINED, RESPECTIVELY.

Method	IoU	mIoU	car (2.88%)	bicycle (0.01%)	motorcycle (0.00%)	truck (0.16%)	other-veh. (0.16%)	person (0.02%)	road (4.96%)	parking (2.51%)	sidewalk (6.43%)	other-grnd. (0.64%)	building (15.67%)	fence (0.96%)	vegetation (4.19%)	terrain (7.10%)	pole (0.22%)	traf.-sign (0.52%)	other-struct. (0.28%)	other-obj. (0.58%)
MonoScene [1]	37.87	12.31	19.3	0.4	0.6	8.0	2.0	0.9	48.4	11.4	28.1	3.2	32.9	3.5	26.2	16.8	6.9	5.7	4.2	3.1
TPVFormer [†] [22]	40.22	13.64	21.6	1.1	1.4	8.1	2.6	2.4	53.0	12.0	31.1	3.8	34.8	4.8	30.1	17.5	7.5	5.9	5.5	2.7
OccFormer [20]	40.27	13.81	22.6	0.7	0.3	9.9	3.8	2.8	54.3	13.4	31.5	3.6	36.4	4.8	31.0	19.5	7.8	8.5	7.0	4.6
VoxFormer ^T [6]	38.76	11.91	17.8	1.2	0.9	4.6	2.1	1.6	47.0	9.7	27.2	2.9	31.2	5.0	29.0	14.7	6.5	6.9	3.8	2.4
Symphonies [7]	44.12	18.58	30.0	1.9	5.9	25.1	12.1	8.2	54.9	13.8	32.8	6.9	35.1	8.6	38.3	11.5	14.0	9.6	14.4	11.3
CGFormer [41]	48.07	20.05	29.9	<u>3.4</u>	4.0	17.6	6.8	6.6	<u>63.9</u>	<u>17.2</u>	40.7	5.5	42.7	8.2	38.8	24.9	16.2	17.5	10.2	6.8
SGN ^T [40]	47.06	18.25	29.0	3.4	2.9	10.9	5.2	3.0	58.1	15.0	36.4	4.4	42.0	7.7	38.2	23.2	<u>16.7</u>	16.4	9.9	5.8
VisHall3D [8]	49.12	<u>20.95</u>	<u>30.8</u>	1.9	<u>6.6</u>	18.0	8.7	8.7	64.4	18.8	41.5	4.5	43.9	<u>9.1</u>	39.8	<u>24.9</u>	16.5	20.7	10.3	8.0
VOIC(Ours)	<u>48.18</u>	21.37	30.9	4.4	7.2	<u>21.0</u>	<u>9.8</u>	<u>8.4</u>	62.6	11.9	<u>41.3</u>	<u>6.1</u>	<u>43.5</u>	11.0	<u>38.9</u>	22.7	17.2	<u>20.1</u>	11.9	<u>9.2</u>

TABLE III
COMPARISON OF INFERENCE TIME AND NUMBER OF PARAMETERS

Method	mIoU (%) [†]	Times (s) [↓]	Params (M) [↓]
MonoScene [1]	11.08	0.274	132.4
OccFormer [20]	13.46	0.338	203.4
VoxFormer [6]	13.35	0.256	57.9
Symphonize [7]	14.89	0.319	59.3
VisHall3D [8]	17.46	0.340	127.8
VOIC(Ours)	18.02	0.243	45.4

TABLE IV
ABLATION STUDY ON ARCHITECTURE, VRLE, AND 2D-TO-3D PROJECTION

Method	VRLE	2D-to-3D Projection	Decoder	IoU (%)	mIoU (%)
Baseline	×	FLoSP	OD	36.86	11.09
1	×	VEFC	OD	44.88	15.88
2	×	VEFC	VD+OD	44.93	16.09
VOIC(Ours)	✓	VEFC	VD+OD	45.53	18.06

which provides more consistent geometric cues for semantic lifting.

Introducing the dual-decoder cascade VD+OD (Method 2), where VEFC is used but VRLE is still omitted and VD is

TABLE V
INTERACTION FLOW ABLATION

Method	Interaction Flow	IoU (%)	mIoU (%)
1	None	44.85	15.56
2	VD → OD	45.33	17.02
VOIC(Ours)	VD ↔ OD	45.53	18.06

supervised using the labels produced by OD, further improves performance to 44.93% IoU and 16.09% mIoU. This confirms that the structured interaction between VD and OD enhances the learning process even without visible-region supervision.

Finally, incorporating the VRLE label as explicit supervision for VD (VOIC, Ours) achieves the best results of 45.53% IoU and 18.06% mIoU. This progression demonstrates the crucial role of VRLE in enabling VD to progressively refine visible-region representations and produce a clear separation between visible and occluded region reconstruction.

Ablation on the Decoder Interaction Flow. Table V summarizes the effect of information exchange between VD and OD. When the two decoders are isolated, the model obtains 15.56% mIoU. Adding a unidirectional link from VD to OD raises the performance to 17.02% mIoU, indicating that visible-region features provide useful priors but

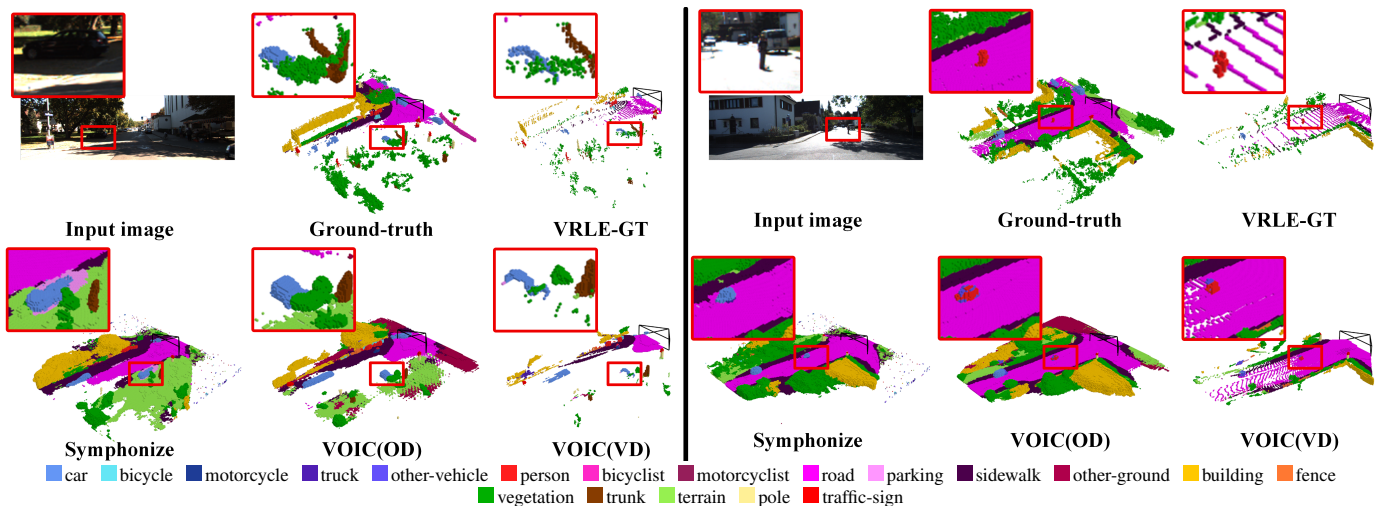


Fig. 6. Qualitative results on the SemanticKITTI validation set. VOIC enhances overall scene classification through high-quality visible-range semantic priors predicted by VD. Shown here is a comparison between VOIC and failure cases of Symphonize [7].

a single forward fusion remains limited. Since VD guides OD through visible-region predictions, it naturally becomes necessary to propagate OD’s global information back to VD to strengthen VD’s feature learning, a capability absent in the unidirectional design. We therefore introduce a reverse link from OD to VD. This feedback brings OD’s global context into VD, enabling mutual refinement and improving the final performance to 17.64% mIoU. Such bidirectional interaction allows both decoders to share complementary cues, benefiting full-scene reconstruction and reducing inconsistencies in the visible regions.

V. CONCLUSION

In this work, the Visible–Occluded Interactive Completion Network (VOIC) is presented as a novel two-stage framework for monocular 3D Semantic Scene Completion (SSC). Unlike prior approaches that treat visible–occluded decoupling as a formal design choice, VOIC is motivated by a critical, previously overlooked problem: incorrect supervision of visible voxels in monocular SSC can systematically degrade global scene completion. By addressing this issue, VOIC enables effective collaborative learning between visible and occluded regions.

The method leverages the Visible Region Label Extraction (VRLE) strategy to generate accurate, visibility-aware supervision for the Visible Decoder (VD), allowing it to produce high-fidelity semantic and geometric priors for observed voxels. Conversely, the Occlusion Decoder (OD) operates under global scene annotations, utilizing these stable priors through an interactive reasoning process to reconstruct the complete 3D scene and effectively resolve ambiguities in occluded spaces.

Additionally, VOIC incorporates a multi-level positional encoding mechanism to enhance geometric alignment during voxel decoding. Experiments on SemanticKITTI and SSCBench-KITTI-360 demonstrate state-of-the-art performance, achieving a geometric IoU of 45.22 and a semantic mIoU of 18.01. By focusing on this problem-driven separation

between visible perception and occluded completion, VOIC establishes a new benchmark for accurate monocular SSC.

REFERENCES

- [1] A.-Q. Cao and R. De Charette, “Monoscene: Monocular 3d semantic scene completion,” in *Proceedings of the IEEE/CVF Conference on Computer Vision and Pattern Recognition*, 2022, pp. 3991–4001.
- [2] R. Cheng, C. Agia, Y. Ren, X. Li, and L. Bingbing, “S3cnet: A sparse semantic scene completion network for lidar point clouds,” in *Conference on Robot Learning*, 2021, pp. 2148–2161.
- [3] Z. Han, S. Li, X. Wang, X. Hu, R. Higashita, and J. Liu, “Multi-path sensory substitution device navigates the blind and visually impaired individuals,” *Displays*, p. 103200, 2025.
- [4] P. Li, R. Zhao, Y. Shi, H. Zhao, J. Yuan, G. Zhou, and Y.-Q. Zhang, “LODE: Locally Conditioned Eikonal Implicit Scene Completion from Sparse LiDAR,” in *2023 IEEE International Conference on Robotics and Automation (ICRA)*, 2023, pp. 8269–8276.
- [5] J. Lee, S. Lee, C. Jo, W. Im, J. Seon, and S.-E. Yoon, “Semcity: Semantic scene generation with triplane diffusion,” in *Proceedings of the IEEE/CVF Conference on Computer Vision and Pattern Recognition*, 2024, pp. 28 337–28 347.
- [6] Y. Li, Z. Yu, C. Choy, C. Xiao, J. M. Alvarez, S. Fidler, C. Feng, and A. Anandkumar, “Voxformer: Sparse voxel transformer for camera-based 3d semantic scene completion,” in *Proceedings of the IEEE/CVF Conference on Computer Vision and Pattern Recognition*, 2023, pp. 9087–9098.
- [7] H. Jiang, T. Cheng, N. Gao, H. Zhang, T. Lin, W. Liu, and X. Wang, “Symphonize 3d semantic scene completion with contextual instance queries,” in *Proceedings of the IEEE/CVF Conference on Computer Vision and Pattern Recognition*, 2024, pp. 20 258–20 267.
- [8] H. Lu, Y. Su, X. Zhang, L. Gao, Y. Xue, and L. Wang, “Vishall3d: Monocular semantic scene completion from reconstructing the visible regions to hallucinating the invisible regions,” in *Proceedings of the IEEE/CVF International Conference on Computer Vision*, 2025, pp. 28 674–28 684.
- [9] J. Behley, M. Garbade, A. Milioto, J. Quenzel, S. Behnke, C. Stachniss, and F. Gall, “Semantickitti: A dataset for semantic scene understanding of lidar sequences,” in *Proceedings of the IEEE/CVF International Conference on Computer Vision*, 2019, pp. 9297–9307.
- [10] Y. Li, S. Li, X. Liu, M. Gong, K. Li, N. Chen, Z. Wang, Z. Li, T. Jiang, and F. Yu, “Sscbench: A large-scale 3d semantic scene completion benchmark for autonomous driving,” in *2024 IEEE/RSJ International Conference on Intelligent Robots and Systems (IROS)*, 2024, pp. 13 333–13 340.
- [11] S. Song, F. Yu, A. Zeng, A. X. Chang, M. Savva, and T. Funkhouser, “Semantic scene completion from a single depth image,” in *Proceedings of the IEEE Conference on Computer Vision and Pattern Recognition*, 2017, pp. 1746–1754.

- [12] X. Chen, K.-Y. Lin, C. Qian, G. Zeng, and H. Li, "3d sketch-aware semantic scene completion via semi-supervised structure prior," in *Proceedings of the IEEE/CVF Conference on Computer Vision and Pattern Recognition*, 2020, pp. 4193–4202.
- [13] J. Li, Y. Liu, D. Gong, Q. Shi, X. Yuan, C. Zhao, and I. Reid, "Rgbd based dimensional decomposition residual network for 3d semantic scene completion," in *Proceedings of the IEEE/CVF Conference on Computer Vision and Pattern Recognition*, 2019, pp. 7693–7702.
- [14] P. Zhang, W. Liu, Y. Lei, H. Lu, and X. Yang, "Cascaded context pyramid for full-resolution 3d semantic scene completion," in *Proceedings of the IEEE/CVF International Conference on Computer Vision*, 2019, pp. 7801–7810.
- [15] X. Wang, Z. Zhu, W. Xu, Y. Zhang, Y. Wei, X. Chi, Y. Ye, D. Du, J. Lu, and X. Wang, "Openoccupancy: A large scale benchmark for surrounding semantic occupancy perception," in *Proceedings of the IEEE/CVF International Conference on Computer Vision*, 2023, pp. 17 850–17 859.
- [16] L. Roldao, R. De Charette, and A. Verroust-Blondet, "Lmscnet: Lightweight multiscale 3d semantic completion," in *2020 International Conference on 3D Vision (3DV)*, 2020, pp. 111–119.
- [17] X. Yan, J. Gao, J. Li, R. Zhang, Z. Li, R. Huang, and S. Cui, "Sparse single sweep lidar point cloud segmentation via learning contextual shape priors from scene completion," in *Proceedings of the AAAI Conference on Artificial Intelligence*, vol. 35, 2021, pp. 3101–3109.
- [18] X. Chang, H. Pan, W. Sun, and H. Gao, "A multi-phase camera-LiDAR fusion network for 3D semantic segmentation with weak supervision," *IEEE Transactions on Circuits and Systems for Video Technology*, vol. 33, no. 8, pp. 3737–3746, 2023.
- [19] Z. Lu, B. Cao, and Q. Hu, "LiDAR-camera continuous fusion in voxelized grid for semantic scene completion," *IEEE Transactions on Circuits and Systems for Video Technology*, 2024.
- [20] Y. Zhang, Z. Zhu, and D. Du, "Occformer: Dual-path transformer for vision-based 3d semantic occupancy prediction," in *Proceedings of the IEEE/CVF International Conference on Computer Vision*, 2023, pp. 9433–9443.
- [21] J. Yao, C. Li, K. Sun, Y. Cai, H. Li, W. Ouyang, and H. Li, "Ndc-scene: Boost monocular 3d semantic scene completion in normalized device coordinates space," in *2023 IEEE/CVF International Conference on Computer Vision (ICCV)*, 2023, pp. 9421–9431.
- [22] Y. Huang, W. Zheng, Y. Zhang, J. Zhou, and J. Lu, "Tri-perspective view for vision-based 3d semantic occupancy prediction," in *Proceedings of the IEEE/CVF Conference on Computer Vision and Pattern Recognition*, 2023, pp. 9223–9232.
- [23] S. Wang, J. Yu, W. Li, W. Liu, X. Liu, J. Chen, and J. Zhu, "Not all voxels are equal: Hardness-aware semantic scene completion with self-distillation," in *Proceedings of the IEEE/CVF Conference on Computer Vision and Pattern Recognition*, 2024, pp. 14 792–14 801.
- [24] H. Xiao, H. Xu, W. Kang, and Y. Li, "Instance-aware monocular 3D semantic scene completion," *IEEE Transactions on Intelligent Transportation Systems*, vol. 25, no. 7, pp. 6543–6554, 2024.
- [25] M. Wang, Y. Ding, Y. Liu, Y. Qin, R. Li, and Z. Tang, "Mixssc: Forward-backward mixture for vision-based 3d semantic scene completion," *IEEE Transactions on Circuits and Systems for Video Technology*, 2025.
- [26] B. Li, J. Deng, W. Zhang, Z. Liang, D. Du, X. Jin, and W. Zeng, "Hierarchical Temporal Context Learning for Camera-Based Semantic Scene Completion," in *Computer Vision – ECCV 2024*, A. Leonardis, E. Ricci, S. Roth, O. Russakovsky, T. Sattler, and G. Varol, Eds., Cham, 2025, vol. 15062, pp. 131–148.
- [27] J. Lin, J. Zhou, W. Xu, R. Xu, C. Wang, S. Chen, K. Fu, Y. Shao, L. Guo, and S. Xu, "CurriFlow: Curriculum-Guided Depth Fusion with Optical Flow-Based Temporal Alignment for 3D Semantic Scene Completion," Oct. 2025.
- [28] H. Lu, Y. Su, X. Zhang, and H. Hu, "One Step Closer: Creating the Future to Boost Monocular Semantic Scene Completion," Jul. 2025.
- [29] S. Chen, W. Sui, B. Zhang, Z. Boukhers, J. See, and C. Yang, "Unleashing Semantic and Geometric Priors for 3D Scene Completion," Aug. 2025.
- [30] F. Gao, Y. Chen, K. Wang, P. Zhou, and J. Lu, "MVFormer: UNet-like Transformer with Mix-Voxel Attention for Camera-Based 3D Semantic Scene Completion," *IEEE Transactions on Circuits and Systems for Video Technology*, 2025.
- [31] D.-H. Pham, D.-D. Nguyen, A. Pham, T. Ho, P. Nguyen, K. Nguyen, and R. Nguyen, "Semi-supervised 3D Semantic Scene Completion with 2D Vision Foundation Model Guidance," in *Proceedings of the AAAI Conference on Artificial Intelligence*, vol. 39, 2025, pp. 6514–6522.
- [32] Z. Yang and Y. Peng, "SPHERE: Semantic-PHysical Engaged REpresentation for 3D Semantic Scene Completion," in *Proceedings of the 33rd ACM International Conference on Multimedia*, Dublin Ireland, Oct. 2025, pp. 7681–7690.
- [33] Y.-W. Tseng, S.-P. Yang, J.-C. Wu, I.-B. Liao, Y.-H. Li, H.-H. Shuai, and W.-H. Cheng, "Memory-Augmented Re-Completion for 3D Semantic Scene Completion," in *Proceedings of the AAAI Conference on Artificial Intelligence*, vol. 39, 2025, pp. 7446–7454.
- [34] F. Li, H. Zhang, H. Xu, S. Liu, L. Zhang, L. M. Ni, and H.-Y. Shum, "Mask dino: Towards a unified transformer-based framework for object detection and segmentation," in *Proceedings of the IEEE/CVF Conference on Computer Vision and Pattern Recognition*, 2023, pp. 3041–3050.
- [35] X. Zhu, W. Su, L. Lu, B. Li, X. Wang, and J. Dai, "Deformable DETR: Deformable Transformers for End-to-End Object Detection," Mar. 2021.
- [36] L.-C. Chen, G. Papandreou, I. Kokkinos, K. Murphy, and A. L. Yuille, "Deeplab: Semantic image segmentation with deep convolutional nets, atrous convolution, and fully connected crfs," *IEEE transactions on pattern analysis and machine intelligence*, vol. 40, no. 4, pp. 834–848, 2017.
- [37] Y. Zhang, Z. Zhu, W. Zheng, J. Huang, G. Huang, J. Zhou, and J. Lu, "Beverse: Unified perception and prediction in birds-eye-view for vision-centric autonomous driving," *arXiv preprint arXiv:2205.09743*, 2022.
- [38] Y. Li, Z. Ge, G. Yu, J. Yang, Z. Wang, Y. Shi, J. Sun, and Z. Li, "Bevdepth: Acquisition of reliable depth for multi-view 3d object detection," in *Proceedings of the AAAI Conference on Artificial Intelligence*, vol. 37, 2023, pp. 1477–1485.
- [39] J. Huang, G. Huang, Z. Zhu, Y. Ye, and D. Du, "BEVDet: High-performance Multi-camera 3D Object Detection in Bird-Eye-View," Jun. 2022.
- [40] J. Mei, Y. Yang, M. Wang, J. Zhu, J. Ra, Y. Ma, L. Li, and Y. Liu, "Camera-based 3d semantic scene completion with sparse guidance network," *IEEE Transactions on Image Processing*, 2024.
- [41] Z. Yu, R. Zhang, J. Ying, J. Yu, X. Hu, L. Luo, S.-Y. Cao, and H.-L. Shen, "Context and geometry aware voxel transformer for semantic scene completion," *Advances in Neural Information Processing Systems*, vol. 37, pp. 1531–1555, 2024.
- [42] I. Loshchilov and F. Hutter, "Decoupled Weight Decay Regularization," Jan. 2019.
- [43] K. He, X. Zhang, S. Ren, and J. Sun, "Deep residual learning for image recognition," in *Proceedings of the IEEE Conference on Computer Vision and Pattern Recognition*, 2016, pp. 770–778.



Zaidao Han received the B.Sc. and M.Sc. degrees from Chongqing University, China, in 2019 and 2022, respectively. He is currently pursuing the Ph.D. degree with the Department of Computer Science and Engineering, Southern University of Science and Technology, China. His research interests include image perception, scene understanding, and assistive interaction methods and devices for visual guidance.



Risa Higashita received the Ph.D. degree in biomedical engineering from Nagoya University, Japan, in 2004. Currently, she is a Visiting Professor with the Department of Computer Science and Engineering, Southern University of Science and Technology, China. Her research interests include medical image processing and ophthalmology.



Jiang Liu (Senior Member, IEEE) received the B.Sc. degree in computer science from the University of Science and Technology of China in 1988, and the M.Sc. and Ph.D. degrees from the National University of Singapore, Singapore, in 1992 and 2004, respectively. He founded the Intelligent Medical Imaging Research Team, which was once the largest ophthalmic medical image processing team in the world, focusing on ophthalmic artificial intelligence research. Currently, he is a Professor with the Department of Computer Science and Engineering, Southern University of Science and Technology, China.